Journal of Materials Chemistry A

Accepted Manuscript

This article can be cited before page numbers have been issued, to do this please use: W. Feng, L. Zhang, Y. Zhang, Y. Yu, Z. Fang, B. Wang, S. Zhang and P. Liu, *J. Mater. Chem. A*, 2017, DOI: 10.1039/C7TA02402A.

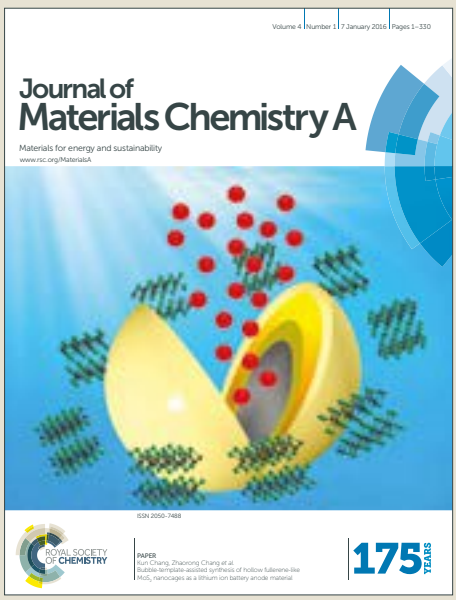

ROYAL SOCIETY OF CHEMISTRY

rsc.li/materials-a

View Article Online
DOI: 10.1039/C7TA02402A

Journal Name

ARTICLE

Near-Infrared-Activated $NaYF_4$: Yb^{3+}, Er^{3+}/Au/CdS for H_2 Production via Photoreforming of Bio-Ethanol: Plasmonic Au as Light Nanoantenna, Energy Relay, Electron Sink and Co-catalyst

Received 00th January 20xx,
Accepted 00th January 20xx

DOI: 10.1039/x0xx00000x

www.rsc.org/

Wenhui Feng, [a] Lulu Zhang, [a] Yan Zhang, [a] Yu Yang, [a] Zhibin Fang, [a] Bo Wang, [a] Shiying Zhang, [b] and Ping Liu*[a]

A sandwich-structured $NaYF_4$: Yb^{3+}, Er^{3+}/Au/CdS architecture, as a up-conversion-involved photocatalyst for H_2 production through photoreforming of renewable bio-ethanol, is constructed successfully. The Au nanoprticles embedding in the $NaYF_4$: Yb^{3+}, Er^{3+}/CdS interface play a quadruplex role to improve the solar utilization efficiency. Firstly, plasmonic Au works as a light nanoantenna to harvest more incident light. Secondly, plasmonic Au acts as an energy relay, that Au SPR-induced Förster resonance energy transfer (FRET) and plasmonic resonance energy transfer (PRET) facilitate synergistically the energy transfer from $NaYF_4$: Yb^{3+}, Er^{3+} to Au to CdS. Thirdly, Au conducts as an electron sink for promoting electron-hole separation. Lastly, Au serves for co-catalyst to activate H_2 evolution from bio-ethanol. The multifunctional Au makes $NaYF_4$: Yb^{3+}, Er^{3+}/Au/CdS exhibit enhanced NIR-driven photocatalytic bio-ethanol reforming activity. Also, $NaYF_4$: Yb^{3+}, Er^{3+}/Au/CdS shows superior photoactivity under simulated sunlight. This unique fabrication has the implications for rationally designing high-efficient solar-energy-harvesting devices.

Introduction

Harvesting the wide spectrum of solar light and achieving an higher solar energy conversion efficiency (SECE) will remain one of the most challenging missions and be highly desirable for photocatalysts.[1, 2] Up to now, most efforts are focused on UV and visible light photocatalysis, while near-infrared (NIR) light which accounts for about 44% of the solar energy is rarely utilized but quite important.[3-18] In order to extended the absorption to NIR region, a nonlinear optical process, known as up-conversion (UC), has been integrated into photocatalytic system.[19-27] Upon near-infrared excitation, certain material containing rare earth is able to generate UC emission fluorescence ranging from UV to NIR. UC material can serve as an medium for transferring NIR light energy to the UV-activated or Vis-activated photocatalyst.

As a kind of promising UC-involved phtocatalysts, UC host material/semiconductor (UC/S) composites show observed NIR-driven photocatalytic performance.[19-21, 24, 25, 28-41] Unfortunately, they usually suffer from small absorption cross-section, which limited UC excitation and luminescent emission efficiency. And in consequence high excitation power densities is needed, which is at odds with the fairly diffuse solar light.[42-45] Besides, the striking difference of refractive index between semiconductor and UC host material would cause strong interface reflection losses and further decrease seriously the incident flux and UC emission intensity, discounting the UC-involved photocatalyst's catalytic efficiency.[31, 46] Therefore the optimization of the UC-involved system is urgent and challenging for lowering pumping threshold in power and improving energy migration efficiency.

Recently, plasmonic nanostructure, which is characterized by their strong interaction with resonant photons through an excitation of surface plasmon resonance (SPR), shows significant promise for conversion of solar to chemical energy due to the outstanding light-trapping and electromagnetic-field-concentrating properties. Particularly, two kinds of efficient non-radiative dipole-dipole energy transfer, Förster resonant energy transfer (FRET) and plasmon resonance energy transfer (PRET), may occur via the enhanced local electromagnetic field on the premise that two dipoles with partially overlapping spectra.[47-51] Alternatively, if plasmonic metal (M) is integrated into UC/S system properly, such nanostructure would not only serve as a light nanoantenna that is beneficial for harvesting the incident light, but also act as an energy relay which extracts energy from UC component via FRET and transfers the accumulated energy to semiconductor via PRET, minimizing the dissipative energy at the UC/S interface. In this case, the issues facing current state-of-the-art UC-involved photocatalysts would be addressed well.

Herein, we proposed a novel model structure UC/M/S in which plasmonic nanostructure acts as an UC/S interface in nanoscale. Considering the premise, the SPR absorbance of M should overlap with UC emission spectra of UC component and absorbance spectra

[a] Research Institute of Photocatalysis, State Key Laboratory of Photocatalysis on Energy and Environment, Fuzhou University, Fuzhou 350002, P. R. China. E-mail: liuping@fzu.edu.cn.
[b] Hunan Provincial Collaborative Innovation Center for Environment and Energy Photocatalysis, Changsha University, Changsha 410022, P. R. China.

Electronic Supplementary Information (ESI) available: [details of experimental procedures, XPS spectra of Au 4f for NYF/Au/CdS composite, tables of gas and Liquid Product yields for photocatalytic bio-ethanol reforming on various samples]. See DOI: 10.1039/x0xx00000x

View Article Online
DOI: 10.1039/C7TA02402A

of semiconductor simultaneously. Yb^{3+}, Er^{3+} co-doped $NaYF_4$ (abbreviated as NYF), Au nanoparticles (NPs), and CdS is selected as the corresponding UC, M and S component, respectively. The unique NYF/Au/CdS nanospheres (NSs) are constructed by a three-step wet-chemical route successfully. The as-synthesized NYF/Au/CdS hybrid is applied to producing H_2 by bio-ethanol photoreforming. Where bio-ethanol is a mixture of ethanol and water (about 12wt% ethanol) with non-toxicity and storage and handling safety. It can be produced renewably by fermentation of biomass sources, such as woody materials, plant crops, agricultural residues, organic fraction of municipal solid waste, *etc*. [52-54] As beneficial by the multifunctional Au NPs, who plays the roles of light nanoantenna, energy relay, electron sink and co-catalyst simultaneously, this unique NYF/Au/CdS composite not only shows improved photocatalytic performance under low-density NIR light irradiation, but also exhibits the soaring H_2 production rate from bio-ethanol photoreforming by using the fairly diffuse simulated sunlight as the only energy source, compared with the bare NYF, NYF/Au and NYF/CdS. Through the implementation of this concept, this model structure provides a new strategy booming efficient and practical NIR-activated photocatalysts.

Experimental

Materials

Yttrium nitrate ($Y(NO_3)_3$, 99.99%), ytterbium nitrate ($Yb(NO_3)_3$, 99.99%) and erbium nitrate ($Er(NO_3)_3$, 99.99%) were purchased from Tianjin Fengyue Chemical Corp. (Tianjin, China). Ethylenediamine tetraacetic acid disodium salt (EDTA, AR), sodium fluoride (NaF, AR), chloroauric acid tetrahydrate ($AuCl_3{\cdot}HCl{\cdot}H_2O$, AR), sodium borohydride ($NaBH_4$, AR), sodium hydroxide (NaOH, AR), L-cysteine (Cys, BR), ethanal absolute (CH_3CH_2OH, AR), sodium sulfate (Na_2SO_4, AR) and N, N-dimethylformamide (DMF, AR) were purchased from Sinopharm Chemical Reagent Co., Ltd. (Shanghai, China). Cadmium nitrate tetrahydrate ($Cd(NO_3)_2{\bullet}4H_2O$) was obtained from Aladdin Industrial Corp. (Shanghai, China). All chemicals were used directly without further purification. Deionized (DI) water used in the synthesis came from local sources.

Synthesis of NYF NSs

The $NaYF_4$: Yb^{3+}, Er^{3+} NSs were synthesized via a modified one-step solvothermal method. Typically, 1.41 mmol $Y(NO_3)_3$, 0.16 mmol $Yb(NO_3)_3$ and 0.032 mmol $Er(NO_3)_3$ were dissolved into 20 mL DI water, forming solution A. 1.6 mmol EDTA was added into 20 mL DI water, and 14.4 mmol NaF was added into 20 mL DI water under vigorous stirring, resulting solution B and C, respectively. After the solution A, B and C were heated to 60 °C, solution B and C was added dropwise into solution A with stirring, respectively. The obtained mixture subsequently was poured into the flask and stirred at 60 °C for a further 1 hr. Then, the resulting suspension was transferred into a 100 mL Teflon-lined autoclave and heated at 180 °C for 3 hr. After cooling to room temperature, the as-prepared NSs were obtained by centrifugation, washing with DI water and absolute ethanol several times and drying at 60 °C in vacuum.

Synthesis of NYF/Au

The Au NPs were deposited onto the surfaces of NYF NSs via a chemical impregnation-reduction process. Briefly, 417 μL $HAuCl_4$ solution (0.049 mM) was dissolved into 20 mL DI water. For displacing Cl^- ions with hydroxyl on the Au precursor, the pH value of the resulting solution was adjusted to about 9.0 with vigorous stirring using a solution of 1.0 M NaOH at room temperature, and then 400 mg NYF NSs were added into this above solution. The obtained suspension was dried in a 60 ºC water bath with stirring, permitting the Au^{3+} completely precipitating on the surface of NYF support. Afterwards, the dried precipitates were immersed into 50 mL 1.0 M $NaBH_4$ aqueous solution to reduce the Au^{3+} to Au^0 for 2 hr, and washed with deionized water to remove Cl^- and other excess ions. Lastly, after the precipitates dried at 60 °C in vacuum overnight, an NYF/Au sample containing about 1 wt.% Au was obtained.

Synthesis of NYF/CdS

0.2 mmol $Cd(NO_3)_2{\bullet}4H_2O$ was mixed with an aqueous solution of *L*-cysteine (10 mL, 0.04 M) and stirred for 30 min. Then, 400 mg NYF power was dispersed into the resulting mixture and stirred for 1 hr. After that, 70 mL absolute ethyl alcohol was added into the obtained suspension, and continue to stir for a further 5 min. The resulting suspension subsequently was transferred into a 100 mL Teflon-lined autoclave and heated at 160 °C for 12 hr. After cooling to room temperature, the as-prepared NYF/CdS, containing about 6.7 wt% CdS, were collected by centrifugation, washing with DI water and absolute ethanol several times and drying at 60 °C in vacuum.

Synthesis of NYF/Au/CdS

0.2 mmol $Cd(NO_3)_2$ was mixed with 10 mL aqueous solution of *L*-cysteine (0.04 M) and stirred for 30 min. Then, 400 mg NYF/Au power was dispersed into the resulting mixture and stirred for 1 hr. After that, 70 mL absolute ethyl alcohol was added into the obtained suspension, and continue to stir for a further 5 min. The resulting suspension subsequently was transferred into a 100 mL Teflon-lined autoclave and heated at 160 °C for 12 hr. After cooling to room temperature, the as-prepared NYF/Au/CdS, containing about 1 wt.% Au and 6.7 wt.% CdS, were collected by centrifugation, washing with DI water and absolute ethanol several times and drying at 60 °C in vacuum.

Characterization

The crystal structures of the as-prepared samples was identified by X-ray diffraction using X-ray powder diffraction (XRD) patterns were carried out on a Bruker D8 ADVANCE X-ray diffractometer, with Cu Ka radiation (l = 0.15418 nm), which operated at 40 kV and 40 mA. The scan rate was 0.5 ($2\theta{\bullet}s^{-1}$). Scanning electron microscopy (SEM) images were obtained using a Nova NanoSEM 230 field-emission scanning electron microscope. Transmission electron microscopy (TEM), high-resolution transmission electron micrographs (HRTEM) and high-angle annular dark field-scanning transmission electron microscope (HAADF-STEM) images were collected with a TecnaiG2F20 S-TWIN with an accelerating voltage of 200 kV. UV-vis-NIR diffuse reflectance spectroscopy (DRS) was measured by a Carry 500 UV-vis spectrophotometer, in which $BaSO_4$ was served as the background. Upconversion emission spectra were recorded by using a FSP920 fluorescence spectrophotometer (Edinburgh Instruments Ltd., UK) under 980 nm excitation using an optical parametric oscillator (OPO) pulsed laser focused on the sample using a lens to obtain a spot with Gaussian intensity distribution (area of 1 mm^2).

View Article Online
DOI: 10.1039/C7TA02402A

The spectra for all samples (0.2 nm for spectral resolution) were collected from powder samples immobilized between two quartz glass slides. All samples were investigated under ambient conditions. The short-circuit transient photocurrent was operated on a ZENNIUM electrochemical workstation (Zahner, Germany) with a conventional three-electrode system. The reference and counter electrodes were Ag/AgCl and Pt plate, respectively, and 0.2 M Na_2SO_4 (pH = 6.8) aqueous solution was used for the electrolyte solution. 10 mg of the as-prepared sample was dispersed in 200 μL N,N-dimethyl formamide (DMF) solution by sonication, and the slurry (40 uL) was then evenly spread onto a indium tin oxide (ITO) conductor glass substrate with an area of 5 mm× 5 mm. Then the glasses covered with samples were dried, and the uncovered parts were painted by insulating epoxy resin. The obtained ITO glass was a working electrode. The NIR light source is obtained by using an 700 nm long-pass filter filtering out the UV-Vis light components of a 300 W xenon lamp. The xenon lamp (300 W) equipped with a 530 nm band-pass filter was used to provide green light source (λ=530±20 nm).

Photocatalytic bio-ethanol reforming reactions

Typically, 15 mg photocatalyst was suspended in bio-ethanol solution (10 mL), which was substituted by a mixture of 1.5 mL ethanol and 8.5 mL water (about 12wt% ethanol). The resulting suspension was poured into a cylindrical quartz reactor (volume ≈ 50 mL), with a gas inlet valve and a gas outlet valve. Then the reactor was pumped into a vacuum and purged with the Ar at atmospheric pressure. The suspension was stirred and exposed to simulated solar light, NIR light or UV-Vis light irradiation, respectively. In experiments where simulated solar light (a 300 W Xe arc lamp equipped with simulated sunlight filter) was used. NIR light source was obtained by using an 700 nm long-pass filter filtering out the UV-Vis light components in simulated solar light. A 300 W Xe arc lamp as the UV-Vis light source where the NIR components were filtered out by wide bandpass infrared filter. The reactor vessel was kept in a water bath at ca. 25 °C throughout the whole experiment. 3 mL gas sample was taken through the outlet valve port, subsequently was injected in a gas chromatograph (Techcomp 7900), equipped with one thermal conductivity detector (TCD) for the quantification of H_2, and a flame ionisation detector (FID) for the quantification of CH_4, CO, CO_2.

Results and discussion

Synthesis and structural properties

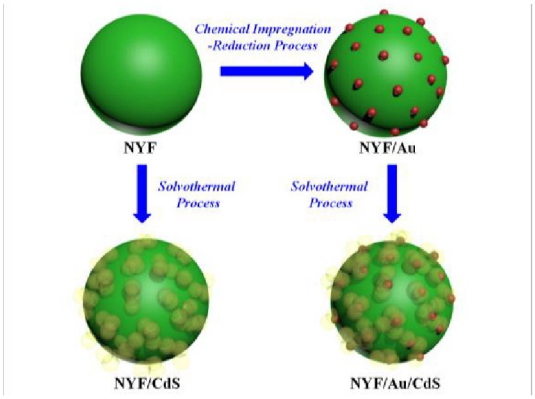

Fig. 1. Schematic illustration of preparations of NYF/Au, NYF/CdS and NYF/Au/CdS composites.

Fig. 1 illustrates the synthesis procedure of the monodisperse NYF/Au/CdS NSs. Firstly, NYF NSs are prepared via the modified hydrothermal method previously reported.[55] Then, Au NPs are deposited uniformly on the NYF NSs through chemical impregnation-reduction process, obtaining NYF/Au composite. Lastly, as-obtained NYF/Au as the support for solvothermal growth of CdS shell, forming NYF/Au/CdS hybrid. Besides, NYF/CdS, as a referential sample, is synthesized by the similar solvothermal process, during which NYF was selected as a template to grow directly CdS. The details of the preparations of all samples are presented in the experimental section.

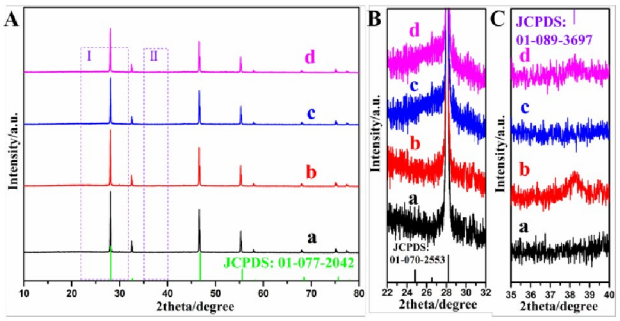

Fig. 2. (A) Typical XRD patterns of NYF (a), NYF/Au (b), NYF/CdS (c), NYF/Au/CdS (d) and enlarged region I and II of the XRD patterns (B, C) of all as-prepared samples.

X-ray diffraction (XRD) patterns of as-prepared samples reveal the characteristics of the cubic phase of $NaYF_4$ (JCPDS Card No. 77-2042) as shown in Fig. 2A. Further, zooming in the red rectangular region I and II, the enlarged XRD patterns are displayed in Fig. 2B and 2C respectively. It can be found that the peaks at 24.8°, 26.5° and 28.2° in the XRD patterns of NYF/CdS and NYF/Au/CdS are corresponding to wurtzite CdS (JCPDS Card No. 70-2553) (100), (002) and (101) lattice plane respectively, while the peak at 38.2° is assigned to Au (111) in the XRD patterns of NYF/Au and NYF/Au/CdS. These results demonstrated that pure NYF is synthesized successfully via hydrothermal method. What's more, Au and CdS could be effectively introduced into the corresponding NYF-based system, without any phase change of NYF through chemical impregnation-reduction process and solvothermal process, respectively.

View Article Online
DOI: 10.1039/C7TA02402A

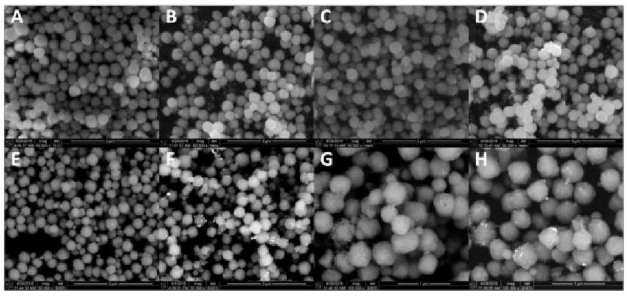

Fig. 3. SEM SE images of NYF (A), NYF/Au (B), NYF/CdS (C), NYF/Au/CdS (D) and BSED images of NYF (E), NYF/Au (F), NYF/CdS (G), NYF/Au/CdS (H).

The scanning electron microscopy (SEM) images (including the secondary electron images (A-D) and backscattered electron diffraction images (E-H)) of all samples are exhibited in Fig. 3. As shown, the morphologies of NYF, NYF/Au, NYF/CdS and NYF/Au/CdS are presented in the form of monodisperse nanospheres. In Fig. 3A and 3E, each NS is smooth-surfaced with a diameter about 100-500 nm. As the SEM images of NYF/Au presented (Fig. 3B and 3F), Au NPs evenly deposit on the surface of NYF NSs (the bright white spots in Fig. 3F represent Au NPs). As displayed in Fig. 3C and 3G, smooth NYF NSs surfaces are roughened with CdS nanocrystals uniformly growing on the surface of NYF NS. Similar appearance is observed in Fig. 3D for NYF/Au/CdS NSs. And Au NPs in NYF/Au/CdS NSs is invisible. But, a few white spots, representing Au NPs, are visible on the surface of NYF/Au/CdS NSs in Fig. 3H. These observations probably reveal that Au NPs mainly exist at the interfaces of NYF/CdS. Meanwhile, it is also proven that the morphology of NYF didn't change visibly during the whole fabrication procedure.

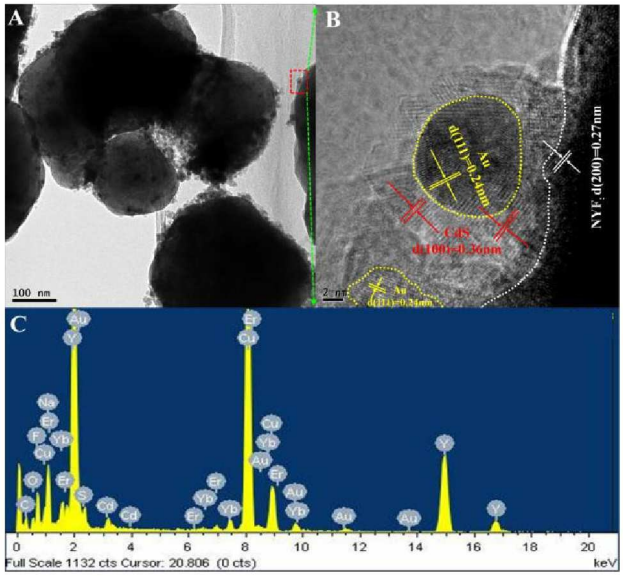

Fig. 4. TEM and HRTEM images of NYF/Au/CdS (A, B) with its EDS spectrum (C).

More detailed structural information of NYF/Au/CdS composite is revealed by transmission electron microscope (TEM) and energy dispersive spectrometry (EDS). Fig. 4A shows that some tiny nanoparticles assemblies are attached to the surface of each NYF NS evenly to form a NYF/Au/CdS NS. Looking closely, it could be found that the outer NPs didn't fully cover the NYF core, keeping a highly open structure. This unique construction may be beneficial for mass transfer. Furthermore, a high-resolution TEM (HRTEM) photograph taken at the red rectangular regions in Fig. 4A displayed in Fig. 4B, three distinct sets of lattice fringes are presented. In the core region, an interlayer spacing of 0.27 nm is observed. This is well-matched with the lattice spacing (d) of (200) lattice plane of cubic $NaYF_4$. An interlayer spacing of 0.36 nm, which is consistent with d(100) of wurtzite CdS, emerges in the superficial NPs. Another noticeable interlayer spacing of 0.24 nm is well-matched with d(111) of fcc Au crystal, which appears in the interface layer. These TEM and HRTEM observations clarify that each NYF NS is coated with CdS, and tiny Au crystals are embedded between NYF and CdS. Besides, EDS spectrum collected on a single NYF/Au/CdS NS further confirms the co-existence of Na, Y, F, Yb, Er, Au, Cd and S elements in a single architecture as shown in Fig. 4C. In addition, the chemical state of Au is also verified by X-ray photoelectron spectroscopy (XPS). As shown in Fig. S1, the Au 4f spectrum for NYF/Au/CdS is identified in two peaks at 83.4 eV and 87.1 eV, which is assigned to metallic Au.[56] It indicates that Au presents in a metallic state, exclusively.

Optical absorption and UC luminescence properties

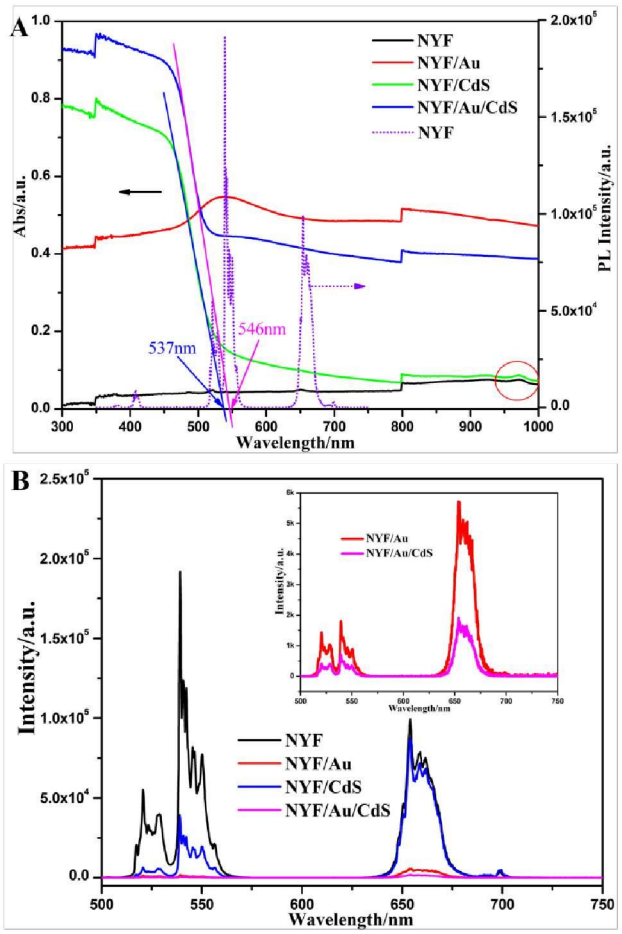

View Article Online
DOI: 10.1039/C7TA02402A

Fig. 5. (A) the UV-vis-NIR absorption spectra of NYF, NYF/Au, NYF/CdS and NYF/Au/CdS (solid line) and the UC luminescence spectrum of NYF upon 980nm NIR excitation (dash line). (B) UC emission spectra of NYF, NYF/Au, NYF/CdS and NYF/Au/CdS (inset: the magnified UC emission spectra of NYF/Au and NYF/Au/CdS).

The optical properties of as-prepared samples are investigated by UV-vis-NIR absorption spectra. As shown in Fig. 5A, bare NYF exhibits only a weak absorption band centered at ~975 nm, which is attributed to the $^2F_{7/2}\rightarrow{}^2F_{5/2}$ transition of Yb^{3+} in the $NaYF_4$ host.[22] With the modification of Au on NYF, one strong broad absorption band located between 490 and 630 nm emerges, which is assigned to the SPR characteristic absorption of Au NPs. Meanwhile, NYF/Au presents an increase in absorption across the entire spectral range compared with the bare NYF, suggesting the plasmonic Au indeed enhances light absorption.[57] The UV-vis-NIR absorption profile of NYF/CdS presents an obvious bandgap absorption of CdS. The band gap is determined to be ~2.3eV (537 nm), using a tangent line to the absorption edge. When CdS NPs grown on the NYF/Au substrate, the Au SPR characteristic absorption and the enhanced bandgap absorption of CdS appear simultaneously. Obviously, the characteristic bandgap absorption band of CdS in NYF/Au/CdS has a slight red-shift compared with one in NYF/CdS, most likely because of the strong electromagnetic coupling between Au and CdS.[58-60] This also further manifests the intimate contact between CdS and Au NPs. Moreover, these UV-vis-NIR spectra intuitively display that there indeed is some overlap between the Au SPR characteristic absorption and bandgap absorption of CdS. To check weather the UC emission spectra of NYF match with both the bandgap absorption of CdS and Au SPR characteristic absorption, which is crucial for NYF/Au/CdS to effectively utilize UC luminescence, the UC emission spectra is also depicted in Fig. 5 (dashed line). Under a 980 nm laser excitation, NYF gives typical green emission ranging from 515 to 565 nm and red emission ranging from 640 to 675 nm in visible light region, those are originated from the ($^2H_{11/2}$, $^4S_{3/2}$)$\rightarrow{}^4I_{15/2}$ and $^4F_{9/2}\rightarrow{}^4I_{15/2}$ transitions of Er^{3+} ions doped in $NaYF_4$ host, respectively.[55] It is obvious that both the SPR characteristic absorption of Au and bandgap absorption of CdS overlap with the UC green emission, but the extent of overlap for the former is greater than the latter. It implies that plasmonic Au can utilize more UC green luminescence than CdS. Meanwhile, neither of them overlaps with the UC red emission.

For further revealing the utilization of UC luminescence in all composites, UC emission spectra under 980 nm excitation of as-prepared samples are exhibited in Fig. 5B. After being covered by CdS, the intensity of green emission decreases slightly, while the red emission changes little. The green emission is reduced mainly via FRET process or radiation-reabsorption processes in NYF/CdS. The unchanged red emission arises from that the energy of red light is lower than the one corresponding bandgap of CdS. It also indicates that the thin CdS layer couldn't attenuate the incident NIR light intensity arriving at the NYF surfaces. The modification of Au NPs results in a remarkable reduction in the intensities of the green emission and red emission. And the decrement of green emission is higher than that of red emission. This phenomenon suggests that the quenching of green emission and red emission in NYF/Au is due to the energy migration from the NYF to plasmonic Au by radiation-reabsorption or FRET mode and scattering mechanism, respectively. For the NYF/Au/CdS hybrid, the intensities of the green and red emission further diminish compared to those of NYF/Au. It indicates that the plasmonic Au and CdS could cooperatively enhance the utilization of UC emission. Which may endue NYF/Au/CdS with good NIR-driven photocatalytic performance.

Bio-ethanol photoreforming performance

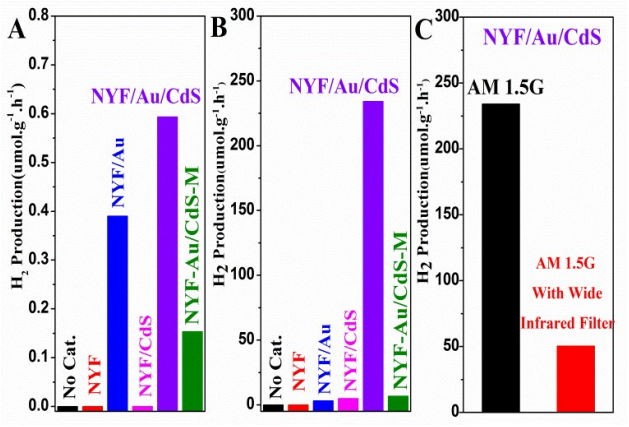

Fig. 6. The photocatalytic bio-ethanol reforming H_2 evolution in the presence of various samples under NIR (A), simulated sunlight (B) and simulated sunlight without NIR component irradiation (C).

To verify our hypothesis, the photocatalytic bio-ethanol reforming H_2 evolution properties of all samples are investigated under the non-coherent NIR light part of simulated sunlight (AM 1.5G). The results are presented in Fig. 6A and Table S1 and S2. As shown in Fig. 6A, the pure bio-ethanol solution with absent of any samples doesn't produce detectable H_2 under NIR irradiation. It excludes the possibility of pure light effects on bio-ethanol photoreforming H_2 production at room temperature. Yet, no H_2 is detected in the presence of NYF or NYF/CdS exposed to the NIR light, indicating that the energetic electrons in NYF cannot be directly utilized in the current photocatalytic system and CdS cannot efficiently harvest the very low-density UC emission fluorescence to generate enough free carriers for bio-ethanol photoreforming H_2 production. However, an observable H_2 production is observed in the presence of NYF/Au, confirming that the energy migrating from the NYF to Au could induce the Au SPR and enable the plasmonic Au to trigger photocatalytic bio-ethanol reforming H_2 production via SPR-induced hot-electron effect or SPR-induced heat effect activating photocatalytic process. As expected, NYF/Au/CdS shows the highest H_2 production rate (0.59 $\mu mol \bullet g^{-1} \bullet h^{-1}$), compared with the NYF, NYF/Au or NYF/CdS. The corresponding apparent quantum efficiency is about 0.00089% under NIR irradiation (λ>700 nm). This further verified the fact that NYF/Au/CdS can high-efficiently utilize the energy migrating from the NYF due to the synergy between plasmonic Au and CdS, resulting a significant NIR-driven photocatalytic performance. Besides, for comparison, the NIR photoactivity of the mechanical mixing sample of NYF and Au/CdS (donated as NYF-Au/CdS-M), with the mass ratio of Au/CdS is 7.7%, is also tested. Au/CdS is prepared by the modified previous method.[61] The detailed experimental processes are presented in Supporting Information. As a result, photocatalytic H_2 production

View Article Online
DOI: 10.1039/C7TA02402A

rate of NYF-Au/CdS-M significantly less than that of NYF/Au/CdS. Which manifests that the enhanced NIR photocatalytic performance of NYF/Au@CdS is attributed to the synergies among all components based on the unique structure, rather than the simply sum of photoactivity of all components. To determine the thermal catalytic contribution of the as-prepared samples to photocatalytic reforming bio-ethanol H_2 evolution, a controlled experiment is conducted in the dark when other experimental conditions are the same. The results are listed in Table S1. No detectable H_2 is released for all samples. It indicates that the thermal catalytic effect doesn't exist at room temperature in the dark for all samples. For the purpose of practical applications, we further study the bio-ethanol photoreforming performances of as-prepared samples under simulated solar light illumination. As shown in Fig. 6B, the pure bio-ethanol solution with absent of any samples doesn't produce detectable H_2 under simulated sunlight irradiation yet. The unique NYF/Au/CdS composite presents the maximum H_2 evolution rate, which is much higher than ones of the others. In order to better reveal that the NIR light components' contribution to solar-light-driven photoactivity, we also measure the bio-ethanol photoreforming H_2 production rate of NYF/Au/CdS under the simulated sunlight irradiation without NIR light part by using a wide infrared filter. When the NIR light is filtered, the H_2 evolution rate declined sharply as shown in Fig. 6C. It indicates that the contribution of NIR is significant for NYF/Au/CdS composite. This surprising result indicates that the combination effect of NYF, Au and CdS components may enhance the NIR-driven photocatalysis and boost the utilization of the solar energy when the unique NYF/Au/CdS is exposed to the sunlight radiation. It also further proves the significance of utilizing the NIR components of sunlight. Among the gaseous products, some minor products detected are CO, CH_4 and CO_2 except for the main product H_2 (data compiled in Table S1). Besides the gaseous products, analysis of liquid products, produced from bio-ethanol over NYF/Au/CdS under the NIR light or simulated sunlight irradiation, is also done (listed in Table S2). In these cases, acetal (i.e. 1,1-diethoxyethane) is the mainly product detected. Which may be formed via the condensation reaction of an acetaldehyde molecule and two ethanol molecules. Acetaldehyde may be the oxidation product from photogenerated holes oxidizing ethanol during photocatalytic process. Traces of acetaldehyde and acetal are detected in the liquid phase, produced from bio-ethanol over NYF/Au/CdS under NIR light irradiation, but unfortunately, the low amounts produced makes accurate quantification difficult. As for quantification of liquid products produced from bio-ethanol over NYF/Au/CdS under the simulated sunlight irradiation, the corresponding acetal, is also the main product detected. The molar ratio of acetal and H_2 is calculated to be ca. 0.71. This value is less than the stoichiometric ratio value of the dissociation of ethanol into acetaldehyde and H_2 via oxidation and reduction reactions, respectively. This result may be due to that a small quantity of acetaldehyde formed decomposes to CH_4, CO or CO_2. In this case, the selectivity of dehydrogenative products is about 71%. The mainly involved reactions are presented as follows:

$$NYF/Au/CdS + hu \rightarrow (NYF/Au/CdS)^* + h^+ + e^- \quad (1)$$

$$CH_3CH_2OH + 2h^+ \rightarrow CH_3CHO + 2H^+ \quad (2)$$

$$2H^+ + 2e^- \rightarrow H_2 \quad (3)$$

$$2CH_3CH_2OH + CH_3CHO \rightarrow CH_3CH(OCH_2CH_3)_2 + H_2O \quad (4)$$

$$CH_3CHO \rightarrow CH_4 + CO + CO_2 \quad (5)$$

Energy transfer

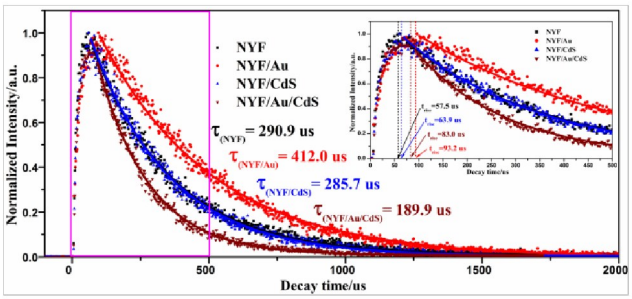

Fig. 7. Time-resolved fluorescence decay curves of Er^{3+} (λ_{em} = 539nm) of NYF, NYF/Au, NYF/CdS and NYF/Au/CdS excited by 980nm laser (inset: the enlarged pink region).

As known, a prerequisite to achieve effective NIR-activated reaction for NYF/Au/CdS is that the high-efficiency energy transfer pathway and process among NYF, Au, and CdS should be guaranteed. To demonstrate the energy transfer process from NYF to Au or CdS, the time-resolved fluorescence dynamic curves of $^4S_{3/2} \rightarrow {}^4I_{15/2}$ transition in Er^{3+} for all samples are measured and the results are shown in Fig. 7. When NYF is coated with CdS, the luminescence rise time and the lifetime of $^4S_{3/2}$ level changes little. It indicates that the energy migration from NYF to CdS is mainly by radiation-reabsorption process in NYF/CdS composites.[32, 62, 63] Comparing with pure NYF and NYF/CdS, Au-modified samples (NYF/Au and NYF/Au/CdS) have a little longer rise times in their temporal evolution curves (Fig. 7 inset), which means that more energy has been transferred from excited Yb^{3+} ions to Er^{3+} ions.[45] This enhanced UC populating processes of Er^{3+} ions in NYF/Au and NYF/Au/CdS further indicates that the plasmonic Au can harvest more incident NIR light to be absorbed by UC component. Moreover, the average decay time of the corresponding excited state increases remarkably after Au NPs depositing (from 290.9 μs to 412.0 μs), which is probably due to the Au SPR-induced photo scattering effect. Most notably, the average decay time of the corresponding excited state in NYF/Au/CdS decreases significantly compared with NYF and NYF/Au. This suggests that the presence of plasmonic Au at the surfaces of NYF NSs creates a non-radiative energy transfer channel from the excited states of Er^{3+} to Au, which is a FRET process, since the fluorescence lifetime of the donor will be unchanged in a radiation-reabsorption process. Such an additional energy transfer process obviously accelerates the relaxation of excited states of Er^{3+}, leading to an increase of the overall energy transition rate and resulting a reduced fluorescence lifetime.[32, 64] This implies that the excited Au SPR in NYF/Au/CdS may decays via a non-radiative mode instead of the scattering mechanism which exists in NYF/Au composite. Because these Au SPR-mediated non-radiative energy transfer processes replace radiation-reabsorption process, the strong interface photon losses are avoided and energy migration efficiency is improved, resulting higher utilization rate of the solar energy.

View Article Online
DOI: 10.1039/C7TA02402A

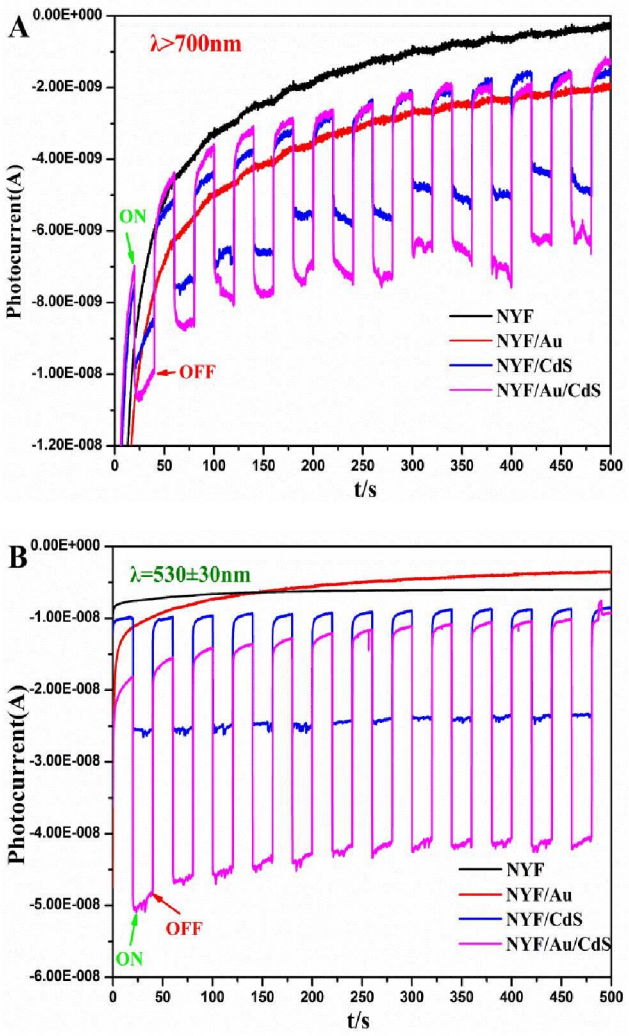

Fig. 8. Short-circuit transient photocurrent response of all samples under NIR irradiation (λ>700nm) (A) and irradiated with λ=530±20 nm(B).

To further reveal the energy migration route and mode between plasmonic Au and CdS, the transient photocurrent responses of all samples under the NIR light irradiation are performed. As depicted in Fig. 8A, both NYF and NYF/Au show a negligible photocurrent under the NIR light irradiation, indicating that plasmonic Au cannot generate conspicuous hot-electrons under the NIR excitation. Combined with the fact that NYF/Au shows evident H_2 production rate, this phenomenon indicates that plasmonic Au could serve as a co-catalyst. NYF/CdS gives an obvious photocurrent under the NIR light irradiation, verifying that CdS shell is capable to absorb some UC green emission and generate photoelectrons. This is consistent with the corresponding UC emission spectra. More remarkable, once Au NPs embedded in NYF/CdS interface, the current density of NYF/Au/CdS increases drastically. These results therefore indicate that Au SPR-induced PRET may enhance significantly electron-hole pairs generation rate for CdS. To further eliminate the contribution of FRET process increasing the photocurrent and confirm the existence of Au SPR-mediated PRET during photocatalytic process in NYF/Au/CdS composite, the photocurrent responses of above-mentioned samples under λ=530±20 nm light irradiation, which can excite directly Au SPR, are also compared. Similar photocurrent behaviors of all samples are displayed in Fig. 8B. These results demonstrate that UC luminescence-induced Au plasmons is indeed decayed by transferring the accumulated energy to CdS and enhancing exciton generation rate in CdS via PRET mechanism rather than hot-electron injection or scattering mechanism. Besides, Au NPs can act as an excellent electron sink to trap free electrons in CdS due to its lower Fermi energy level than the conduction band position of CdS.[65] Consequently, this would greatly accelerate the separation of photogenerated electron-hole pairs with more electrons transferring to highly active plasmonic Au and holes leaving in CdS. The results make the energy migration mode and route between Au and CdS clear. That is, after the Au SPR is excited, the optically extracting energy is transferred from plasmonic metal to semiconductor via PRET process, inducing more free carriers in CdS. Subsequently, the photoinduced electrons are scavenged by Au NPs and photoexcited holes are left in CdS shell. Finally, the separated holes and electrons could participate in related chemical transformation.

Mechanism of the enhanced NIR-driven photoactivity

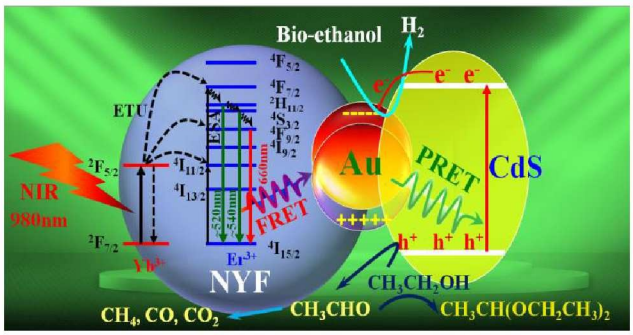

Scheme 1. Illustrative diagrams of energy transfer among NYF, Au and CdS and the process of the bio-ethanol photoreforming H_2 evolution under NIR irradiation.

Based on the above observations and discussions for the NIR-driven bio-ethanol photoreforming reaction, the possible energy migration route and photoactivity enhanced mechanism in NYF/Au/CdS are illustrated in Scheme 1. Firstly, NYF absorbs the concentrated incident NIR light, and Yb^{3+} ions are excited from their ground state ($^2F_{7/2}$ level) to excited state ($^2F_{5/2}$ level). Subsequently, Yb^{3+} ions in exited state dominantly leads the Er^{3+} ions being excited to their high-energy levels by energy-transfer upconversion (ETU) from the excited Yb^{3+} ions to Er^{3+} ions. Meanwhile, the excited-state absorption (ESA) is also exist. Then, the energy of the excited state $^2H_{11/2}$ and $^4S_{3/2}$ level of Er^{3+} is transferred directly to Au via FRET process, exciting Au SPR, since these two excited state levels match well with the Au NPs SPR absorbance. Afterwards, a concentrated electromagnetic field is induced near surface of Au nanostructures and the electronmagnetic field mediated PRET between Au and CdS occurs on the premise that the overlapping absorbance spectra of CdS and Au SPR. Because of the enhanced local elctronmagnetic field, the PRET process can directly trigger more electron-hole pairs in CdS. Then, the free electrons in the CB of CdS are captured by Au NPs, while the holes transfer to the surface of CdS nanocrystals.

View Article Online
DOI: 10.1039/C7TA02402A

This could effectively suppress the recombination of carriers in CdS. Moreover, the plasmonic Au may also act as a co-catalyst and provide active sites for bio-ethanol photoreforming H_2 evolution. Eventually, the separated electrons and holes can react with the adsorbed CH_3CH_2OH on the surface of Au and CdS, mainly forming H_2 and CH_3CH_2O. The interface between metallic Au and CdS may play a key role in bio-ethanol photoreforming reaction mechanism.[66] More experiments for revealing the mechanism of photocatalytic bio-ethanol reforming producing H2 and corresponding carbonyl compounds over NYF/Au/CdS photocatalyst are ongoing.

Conclusions

In summary, on the one hand, plasmonic Au NPs sandwiched between NYF and CdS play as a light concentrator and an energy relay for overcoming the small absorption cross-section limit and interfacial energy loss issue facing the current state-of-the-art UC-involved photocatalysts. On the other hand, Au NPs also play the roles of electron sink and co-catalyst to promoting carrier separation and lowering catalytic reaction barrier for the related chemical transformation. On account of the multiple mediator effects of plasmonic Au, the NYF/Au@CdS composite exhibits obviously enhanced bio-ethanol photoreforming activity under low-density NIR light and the simulated solar light irradiation. The established UC/M/S photocatalytic system offers a new strategy for developing effective and robust NIR-driven UC-involved photocatalysis systems, that will greatly improve solar-energy utilization efficiency.

Acknowledgements

The authors acknowledge the support from National Natural Science Foundation of China (21273035, 21173046 and 21473031), the funding under National Key Technologies R & D Program of China (2014BAC13B03), National Basic Research Program of China (973 Program: 2013CB632405), and Science & Technology Plan Project of Fujian Province (2014Y2003) .

References

1 J. Tian, Y. Sang, G. Yu, H. Jiang, X. Mu and H. Liu, *Adv. Mater.*, 2013, **25**, 5075-5080.
2 S. K. Cushing, J. Li, F. Meng, T. R. Senty, S. Suri, M. Zhi, M. Li, A. D. Bristow and N. Wu, *J. Am. Chem. Soc.*, 2012, **134**, 15033-15041.
3 R. Yan, M. Chen, H. Zhou, T. Liu, X. Tang, K. Zhang, H. Zhu, J. Ye, D. Zhang and T. Fan, *Sci. Rep.*, 2016, **6**, 20001.
4 T. Hisatomi, J. Kubota and K. Domen, *Chem. Soc. Rev.*, 2014, **43**, 7520-7535.
5 A. S. Cherevan, P. Gebhardt, C. J. Shearer, M. Matsukawa, K. Domen and D. Eder, *Energy Environ. Sci.*, 2014, **7**, 791-796.
6 G. Chen, H. Agren, T. Y. Ohulchanskyy and P. N. Prasad, *Chem. Soc. Rev.*, 2015, **44**, 1680-1713.
7 D. J. Martin, G. Liu, S. J. Moniz, Y. Bi, A. M. Beale, J. Ye and J. Tang, *Chem. Soc. Rev.*, 2015, **44**, 7808-7828.
8 Q. Wang, T. Hisatomi, Q. Jia, H. Tokudome, M. Zhong, C. Wang, Z. Pan, T. Takata, M. Nakabayashi, N. Shibata, Y. Li, I. D. Sharp, A. Kudo, T. Yamada and K. Domen, *Nat. Mater.*, 2016, **15**, 611-615.
9 T. Ohno, L. Bai, T. Hisatomi, K. Maeda and K. Domen, *J. Am. Chem. Soc.*, 2012, **134**, 8254-8259.
10 F. Lei, L. Zhang, Y. Sun, L. Liang, K. Liu, J. Xu, Q. Zhang, B. Pan, Y. Luo and Y. Xie, *Angew. Chem. Int. Ed.*, 2015, **54**, 9266-9270.
11 C. Pan, T. Takata, M. Nakabayashi, T. Matsumoto, N. Shibata, Y. Ikuhara and K. Domen, *Angew. Chem. Int. Ed.*, 2015, **54**, 2955-2959.
12 Y. Zheng, L. Lin, B. Wang and X. Wang, *Angew. Chem. Int. Ed.*, 2015, **54**, 12868-12884.
13 J. L. White, M. F. Baruch, J. E. Pander Iii, Y. Hu, I. C. Fortmeyer, J. E. Park, T. Zhang, K. Liao, J. Gu, Y. Yan, T. W. Shaw, E. Abelev and A. B. Bocarsly, *Chem. Rev.*, 2015, **115**, 12888-12935.
14 A. Sinhamahapatra, J.-P. Jeon and J.-S. Yu, *Energy Environ. Sci.*, 2015, **8**, 3539-3544.
15 J. Tian, Y. Leng, Z. Zhao, Y. Xia, Y. Sang, P. Hao, J. Zhan, M. Li and H. Liu, *Nano Energy*, 2015, **11**, 419-427.
16 J. Hou, H. Cheng, C. Yang, O. Takeda and H. Zhu, *Nano Energy*, 2015, **18**, 143-153.
17 X. Meng, T. Wang, L. Liu, S. Ouyang, P. Li, H. Hu, T. Kako, H. Iwai, A. Tanaka and J. Ye, *Angew. Chem. Int. Ed.*, 2014, **53**, 11478-11482.
18 J. Ren, S. Ouyang, H. Xu, X. Meng, T. Wang, D. Wang and J. Ye, *Adv. Energy Mater.*, 2017, **7**, 1601657.
19 W. Yang, X. Li, D. Chi, H. Zhang and X. Liu, *Nanotechnology*, 2014, **25**, 482001.
20 Z. Li, C. Li, Y. Mei, L. Wang, G. Du and Y. Xiong, *Nanoscale*, 2013, **5**, 3030-3036.
21 W. Wang, M. Ding, C. Lu, Y. Ni and Z. Xu, *Appl. Catal. B: Environ.*, 2014, **144**, 379-385.
22 Z. Xu, M. Quintanilla, F. Vetrone, A. O. Govorov, M. Chaker and D. Ma, *Adv. Funct. Mater.*, 2015, **25**, 2950-2960.
23 H.-i. Kim, O. S. Kwon, S. Kim, W. Choi and J.-H. Kim, *Energy Environ. Sci.*, 2016, **9**, 1063-1073.
24 M. Tou, Y. Mei, S. Bai, Z. Luo, Y. Zhang and Z. Li, *Nanoscale*, 2016, **8**, 553-562.
25 W. Wang, Y. Li, Z. Kang, F. Wang and J. C. Yu, *Appl. Catal. B: Environ.*, 2016, **182**, 184-192.
26 B. Zhou, B. Shi, D. Jin and X. Liu, *Nat. Nanotechnol.*, 2015, **10**, 924-936.
27 X. Guo, W. Di, C. Chen, C. Liu, X. Wang and W. Qin, *Dalton Trans.*, 2014, **43**, 1048-1054.
28 W. Qin, D. Zhang, D. Zhao, L. Wang and K. Zheng, *Chem. Commun.*, 2010, **46**, 2304-2306.
29 S. Obregón, A. Kubacka, M. Fernández-García and G. Colón, *J. Catal.*, 2013, **299**, 298-306.
30 S. Obregon and G. Colon, *Chem. Commun.*, 2012, **48**, 7865-7867.
31 B. Zheng, Q. Guo, D. Wang, H. Zhang, Y. Zhu, S. Zhou and R. J. Xie, *J. Am. Chem. Soc.*, 2015, **98**, 136-140.
32 Y. Tang, W. Di, X. Zhai, R. Yang and W. Qin, *ACS Catal.*, 2013, **3**, 405-412.
33 Y. Zhang and Z. Hong, *Nanoscale*, 2013, **5**, 8930-8933.
34 Y. Ma, H. Liu, Z. Han, L. Yang and J. Liu, *J. Mater. Chem. A*, 2015, **3**, 14642-14650.
35 S. Obregón and G. Colón, *Appl. Catal. B: Environ.*, 2014, **152-153**, 328-334.
36 S. Obregón and G. Colón, *Appl. Catal. B: Environ.*, 2014, **158-159**, 242-249.
37 W. Su, M. Zheng, L. Li, K. Wang, R. Qiao, Y. Zhong, Y. Hu and Z. Li, *J. Mater. Chem. A*, 2014, **2**, 13486.

View Article Online
DOI: 10.1039/C7TA02402A

38 X. Li, H. Ren, Z. Zou, J. Sun, J. Wang and Z. Liu, *Chem. Commun.*, 2016, **52**, 453-456.
39 S. Ganguli, C. Hazra, M. Chatti, T. Samanta and V. Mahalingam, *Langmuir*, 2016, **32**, 247-253.
40 D. Yin, L. Zhang, X. Cao, Z. Chen, J. Tang, Y. Liu, T. Zhang and M. Wu, *Dalton Trans.*, 2016, **45**, 1467-1475.
41 C. Li, F. Wang, J. Zhu and J. C. Yu, *Appl. Catal. B: Environ.*, 2010, **100**, 433-439.
42 F. Auzel, *Chem. Rev.*, 2004, **104**, 139-173.
43 W. Feng, L. D. Sun and C. H. Yan, *Chem. Commun.*, 2009, 4393-4395.
44 P. Yuan, Y. H. Lee, M. K. Gnanasammandhan, Z. Guan, Y. Zhang and Q. H. Xu, *Nanoscale*, 2012, **4**, 5132-5137.
45 N. Liu, W. Qin, G. Qin, T. Jiang and D. Zhao, *Chem. Commun.*, 2011, **47**, 7671-7673.
46 S. Zhou, T. Matsuoka, Y. Shimotsuma, M. Sakakura, M. Nishi, Z. Hong, J. Qiu, K. Hirao and K. Miura, *Nanotechnology*, 2012, **23**, 465704.
47 S. Linic, U. Aslam, C. Boerigter and M. Morabito, *Nat. Mater.*, 2015, **14**, 567-576.
48 S. Linic, P. Christopher and D. B. Ingram, *Nat. Mater.*, 2011, **10**, 911-921.
49 C. Clavero, *Nat. Photonics*, 2014, **8**, 95-103.
50 J. Li, S. K. Cushing, F. Meng, T. R. Senty, A. D. Bristow and N. Wu, *Nat. Photonics*, 2015, **9**, 601-607.
51 S. C. Warren and E. Thimsen, *Energy Environ. Sci.*, 2012, **5**, 5133-5146.
52 M. Ni, D. Y. C. Leung and M. K. H. Leung, *Int. J. Hydrogen Energy*, 2007, **32**, 3238-3247.
53 Y. Sun and J. Y. Cheng, *Bioresource Technol.*, 2002, **83**, 1-11.
54 R. M. Navarro, M. C. Sánchez-Sánchez, M. C. Alvarez-Galvan, F. d. Valle and J. L. G. Fierro, *Energy Environ. Sci.*, 2009, **2**, 35-54.
55 Y. Sun, Y. Chen, L. Tian, Y. Yu, X. Kong, J. Zhao and H. Zhang, *Nanotechnology*, 2007, **18**, 275609.
56 Y. Azizi, C. Petit and V. Pitchon, *J. Catal.*, 2010, **269**, 26-32.
57 A. Polman and H. A. Atwater, *Nat. Mater.*, 2012, **11**, 174-177.
58 H. Zhao, M. Wu, J. Liu, Z. Deng, Y. Li and B.-L. Su, *Appl. Catal. B: Environ.*, 2016, **184**, 182-190.
59 H. Tada, T. Mitsui, T. Kiyonaga, T. Akita and K. Tanaka, *Nat. Mater.*, 2006, **5**, 782-786.
60 J. Fang, L. Xu, Z. Zhang, Y. Yuan, S. Cao, Z. Wang, L. Yin, Y. Liao and C. Xue, *ACS Appl. Mater. Inter.*, 2013, **5**, 8088-8092.
61 W.-T. Chen, T.-T. Yang and Y.-J. Hsu, *Chem. Mater.*, 2008, **20**, 7204-7206.
62 X. Guo, W. Song, C. Chen, W. Di and W. Qin, *Phys. Chem. Chem. Phys.*, 2013, **15**, 14681-14688.
63 M. Yao, X. Zhang, L. Ma, W. Chen, A. G. Joly, J. Huang and Q. Wang, *J. Appl. Phys.*, 2010, **108**, 103104.
64 H. Jia, S. H. Zheng, C. Xu, W. B. Chen, J. C. Wang, X. F. Liu and J. R. Qiu, *Adv. Energy Mater.*, 2015, **5**, n/a-n/a.
65 T.-T. Yang, W.-T. Chen, Y.-J. Hsu, K.-H. Wei, T.-Y. Lin and T.-W. Lin, *J. Phys. Chem. C*, 2010, **114**, 11414-11420.
66 Z. Chai, T. T. Zeng, Q. Li, L. Q. Lu, W. J. Xiao and D. Xu, *J. Am. Chem. Soc.*, 2016, **138**, 10128-10131.

View Article Online
DOI: 10.1039/C7TA02402A

Table of contents entry

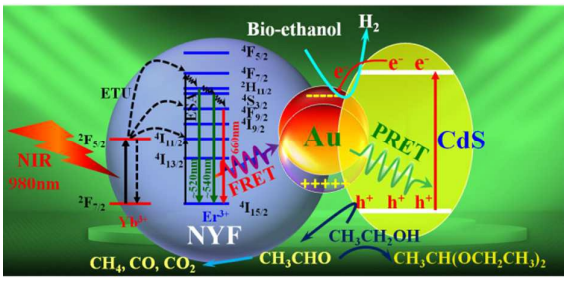

A sandwich-structured $NaYF_4$: Yb^{3+}, Er^{3+}/Au/CdS architecture delivers enhanced photocatalytic bio-ethanol reforming activity under low-density NIR light irradiation.